J Solid State Electrochem (2005) 9: 363–370
DOI 10.1007/s10008-005-0653-y

ORIGINAL PAPER

Zuo-Feng Chen · Yan-Xia Jiang · Ye Wang
Jin-Mei Xu · Lan-Ying Jin · Shi-Gang Sun

Electrocatalytic oxidation of carbon monoxide and methanol at Pt nanoparticles confined in SBA-15: voltammetric and in situ infrared spectroscopic studies

Received: 13 September 2004 / Revised: 9 November 2004 / Accepted: 28 January 2005 / Published online: 12 May 2005

Abstract Electrocatalytic oxidation of carbon monoxide and methanol at Pt nanoparticles confined in mesoporous molecular sieve SBA-15 was studied by using cyclic voltammetry and in situ FTIR spectroscopy. Cyclic voltammetric studies revealed that the Pt nanoparticles confined in SBA-15 exhibit a high activity in the presence of hydrated phase consisting of SiO_2 in the SBA-15. In situ FTIR spectroscopy results discovered that IR absorption of CO adsorbed on Pt nanoparticles confined in SBA-15 has been enhanced 11-fold, and the full-width at half-maximum of the CO band is significantly increased, in comparison with IR feature of CO adsorbed on a bulk Pt electrode. The linearly adsorbed CO species is the only intermediate derived from dissociative adsorption of methanol, which is more readily oxidized to form CO_2 in the aid of the active oxide in SBA-15.

Keywords SBA-15 molecular sieve · Pt nanoparticles · CO · Methanol · Electrocatalytic oxidation

Introduction

Electrocatalytic oxidation of methanol on different Pt electrodes has been widely studied because of its importance in both fundamental electrocatalysis and applications in direct fuel cells. It is generally agreed that, the anodic oxidation of methanol occurs through a dual-path reaction mechanism, i.e., the path via reactive intermediates and the path via poisoning intermediates. Presently, the key issue mainly consists in both the low electrocatalytic activities and easy poisoning of the anode catalysts [1]. In order to improve the catalytic properties and to minimize the poisoning effect of anode catalysts evoked by the intermediates of methanol dissociative adsorption, composite catalytic systems, such as Pt/C [2], Pt alloy [3], Pt oxides [4], Polymer (Pt)/GC [5–7] etc, were investigated. Early studies have already shown up that the enhanced electrocatalytic activity might be attributed to the fitting diameter and the uniform dispersion of Pt microparticles [2, 6]. SBA-15 [8] is a new type of mesoporous molecular sieve or silica with a highly ordered hexagonal arrangement of cylindrical mesopores. This material possesses a narrow pore size distribution and thicker pore walls that accounts for a higher hydrothermal stability than that of the molecular sieve MCM-41 [9]. In addition, different kinds of metals can be incorporated into SBA-15 by direct synthesis [10] or post synthesis methods [11]. These properties make the SBA-15 potentially useful as a supporting material for catalytic applications. In the present paper, Pt nanoparticles confined in SBA-15 silica were prepared, and the electrocatalytic oxidation of CO and methanol on the nanomaterials were studied by using cyclic voltammetry, programmed potential step technique and in situ FTIR spectroscopy.

This paper is dedicated to Professor G. Horanyi on the occasion of his 70th birthday and in recognition of his outstanding contribution to electrochemistry

Z.-F. Chen · Y.-X. Jiang (✉) · Y. Wang · J.-M. Xu
L.-Y. Jin · S.-G. Sun
Department of Chemistry,
State Key Lab for Physical
Chemistry of Solid Surfaces,
Xiamen University, 361005 Xiamen,
People's Republic of China
E-mail: yxjiang@xmu.edu.cn
Tel.: +86-592-2180181
Fax: +86-592-2183047
E-mail: sgsun@xmu.edu.cn

Experimental

Synthesis of SBA-15

SBA-15 used in this work was synthesized in a similar manner as reported elsewhere [12, 13]. Typically, a homogeneous mixture comprised of Pluronic P123 triblock copolymers ($EO_{20}PO_{70}EO_{20}$) and tetraethyl

orthosilicate (TEOS) in hydrochloric acid was stirred at 308 K for 24 h and further treated at 370 K for 24 h to obtain as-synthesized SBA-15. The as-synthesized SBA-15 was separated by filtration, followed by repeated washing with deionized water, drying in vacuum at 313 K and calcinating at 923 K for 6 h. The pore diameter of SBA-15 synthesized in above manner is ca. 5 nm, as well as the BET surface area is ca. 645 m^2 g^{-1} and the pore volume is ca. 0.80 cm^3 g^{-1}.

Preparation of electrodes

K_2PtCl_6 was introduced into SBA-15 by impregnating the SBA-15 in a solution of K_2PtCl_6 for 48 h. The mixture was heated in air at 353 K for 8 h to vaporize water, following at 473 K for 24 h, and then it was washed with Millipore water. The process was repeated thrice. The material thus prepared was dispersed through magnetic force stirring in a solution of dichlorethane containing polyvinyl chloride (PVC) to form a suspension. A glassy carbon (GC) electrode was polished mechanically with alumina from 1.0 μm down to 0.05 μm followed by sonication to remove debris. A defined quantity of the suspension was applied to the clean surface of GC substrate to form a thin film electrode, which was dried in air for about 20 min. The K_2PtCl_6 embedded in SBA-15 was reduced to produce Pt nanoparticles in 0.1 M H_2SO_4 solution through potential cyclic scanning between 0.10 V and −0.25 V. The prepared electrode was designated as Pt-SBA-15/GC.

In situ FTIR spectroscopy

In situ FTIR spectroscopic measurements were carried out on a Nexus 870 FTIR spectrometer (Nicolet) equipped with an EverGlo IR source and a liquid nitrogen-cooled MCT-A detector. An electrochemical IR cell of a thin layer configuration was employed. A CaF_2 disk was used as IR window, and the electrode was pushed against the window to form a thin layer during FTIR measurements. The multi-step FTIR (MS-FTIR) spectroscopy procedure [14] was used in the present study. In this procedure, a series of single-beam spectra at sample potentials (E_S) and a single-beam spectrum at reference potential (E_R) were collected, respectively. The resulting spectra were calculated using

$$\Delta R/R = (R(E_S) - R(E_R))/R(E_R) \quad (1)$$

where $R(E_S)$ and $R(E_R)$ are single-beam spectra collected at sample potential E_S and reference potential E_R, respectively. According to Eq. 1, a negative-going band can be ascribed to IR absorption at E_S and a positive-going band is ascribed to IR absorption at E_R. Each single-beam spectrum was recorded by collecting and co-adding 400 interferograms at a spectral resolution of 8 cm^{-1}.

Other experimental conditions

The experiments of X-ray diffraction (XRD) were carried out on a diffractometer of X' pert PRO (Japan) with K_α of Cu target as radiant point. The cyclic voltammetric and programmed potential step studies were carried out on a CHI-660A electrochemical workstation (Chenhua Corporation, Shanghai China). All chemicals were analytical grade. The solutions were prepared with Millipore water. Before each measurement, the solution was degassed by bubbling pure N_2 gas to the cell for 10 min. The CO adsorbed on Pt-SBA-15/GC electrode (denoted as CO_{ad}-Pt-SBA-15/GC) was obtained by purging CO of high-purity (99.95%) along with potential cyclic scanning between 0.0 V and −0.25 V for 20 min. The solution CO species were then removed by purging pure N_2 gas. The reference electrode used was a saturated calomel electrode (SCE), and potentials reported in the present paper are those with respect to the SCE scale. The geometric surface area of electrode was used to calculate current density, except the comparison of methanol oxidation transients on the Pt-SBA-15/GC and a Pt polycrystalline bead electrode in Fig. 6, where the effective surface area of the electrode was determined from under-potential deposition (UPD) of a monolayer of hydrogen (∼210 μC cm^{-2}), as commonly used by other authors [15]. The performance of Pt-SBA-15/GC electrode for CO and methanol oxidation was generally evaluated at 50 mV s^{-1} in a solution of 0.1 M H_2SO_4 and 0.1 M H_2SO_4 + 0.05 M CH_3OH respectively, unless stated otherwise. All experiments were carried out at room temperature.

Results and discussion

XRD characterization

Figure 1 shows XRD spectra of SBA-15 silica (a) without and (b) with K_2PtCl_6 loading. Three diffraction peaks appear in the two spectra, which are attributed to the characteristic diffraction peaks of (100),(110) and (200) for SBA-15, respectively [8, 12, 13]. The XRD result demonstrates that the SBA-15 still presents the structure of typical hexangular phase in $2\theta = 0.5° \sim 2°$ after loading K_2PtCl_6, indicating that the SBA-15 retains the regular mesoporous structure well. In addition, it is worthy to note that, after impregnating K_2PtCl_6 into SBA-15, the peaks have slightly shifted positively, the intensity of the peaks has decreased to a certain extent, while the full width at half-maximum (FWHM) of the peaks that is normalized by height has increased. These three features are attributed to the shrinking of the mesoporous channel, implying that K_2PtCl_6 has been introduced into the channel of SBA-15 successfully.

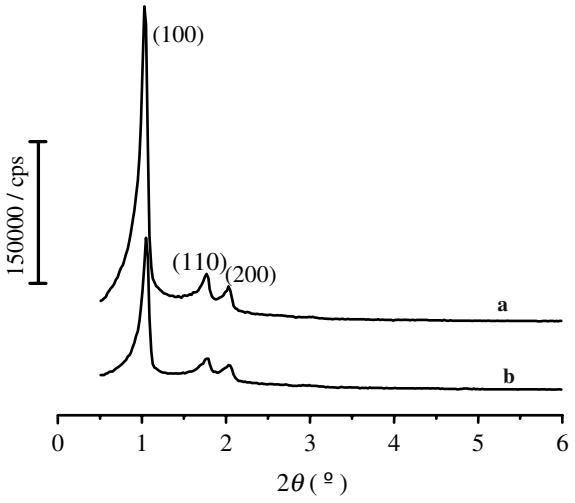

Fig. 1 XRD spectra of SBA-15 silica **a** without **b** with K_2PtCl_6 loading

Electrocatalytic oxidation of adsorbed CO

Figure 2 shows the stable cyclic voltammograms (CVs) of SBA-15/GC, Pt-SBA-15/GC, and CO_{ad}-Pt-SBA-15/GC in 0.1 M H_2SO_4 solution. The CV curve of Fig. 2(a) displays only double layer charging current. Well-known CV features of a Pt polycrystalline electrode can be observed from Fig. 2(b). Two distinct pairs of current peak between −0.25 V and 0.05 V are the characteristic CV features for hydrogen adsorption–desorption. Pt oxide is formed in the positive-going potential sweep (PGPS) up to potentials above 0.6 V. In the reverse scan, a reduction current peak of Pt oxide is seen at 0.45 V. It can be observed from Fig. 2(c) that the hydrogen adsorption–desorption current is suppressed when the electrode surface is

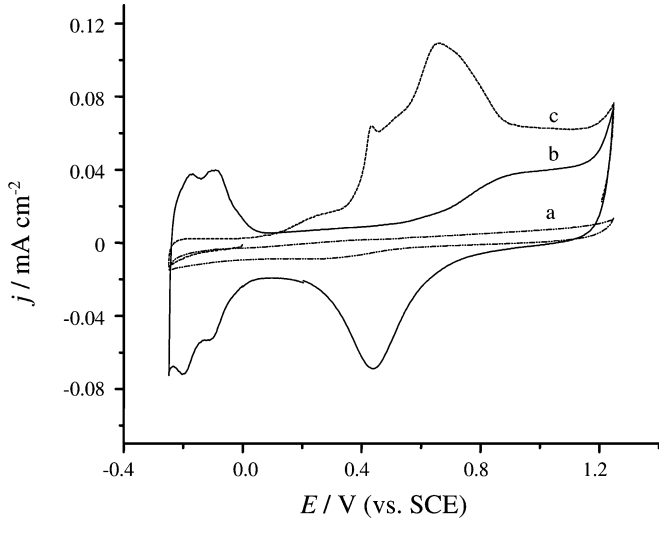

Fig. 2 Cyclic voltammograms of **a** SBA-15/GC, **b** Pt-SBA-15/GC, and **c** the oxidation of adsorbed CO on Pt-SBA-15/GC, in 0.1 M H_2SO_4, sweep rate 50 mV s^{-1}

covered with CO. The onset potential of CO_{ad} oxidation is measured at about 0.10 V, which is about 0.40 V lower than that measured in the CVs of a bulk Pt electrode [16, 17]. This fact indicates that the Pt-SBA-15/GC electrode possesses a good electrocatalytic activity for CO_{ad} oxidation. Moreover, the oxidation of CO_{ad} occurs in a wide potential region lying between 0.1 V and 0.8 V. Such CV features may be attributed to the following two factors: first, CO can adsorb in SBA-15 channel. Such porous materials are often used as adsorbent for gas [18, 19]. Therefore, after the active Pt sites are empty out due to CO_{ad} oxidation, the gaseous CO in SBA-15 channel will diffuse to Pt nanoparticles and absorb on the active Pt sites quickly. It will, on the one hand, make CO oxidation occur in a wide potential range; on the other hand, it will also make the charge of CO oxidation large as compared to the charge of hydrogen adsorption–desorption on a smooth bulk Pt electrode. Second, CO can adsorb on different Pt sites. Besides the primary hexagonal cylindrical channel, SBA-15 still possesses a lot of micropores or microchannels that have put up bridges between the primary channels [20]. When Pt nanoparticles are embedded in the above different locations, it will also ultimately result in the different oxidation potentials for CO_{ad} in a large range. The CO_{ad} oxidation current disappears after one potential cyclic scanning, indicating that CO_{ad} can be easily oxidized on Pt-SBA-15/GC electrode. This may be attributed to the hereinafter two factors. First, there is a lot of silicon-hydroxyl (Si-OH) in the inner surface of SBA-15 channel, which could have a strong interaction with Pt nanoparticles, so it may serve as the active oxide species for CO_{ad} oxidation. Second, SBA-15 possesses mesoporous channels, the CO_2 derived from the oxidation of CO_{ad} can diffuse easily from the SBA-15 to bulk solution. This is different from the microporous zeolite, in which the restriction of the supercage window in zeolite has resulted in the difficulty of CO_{ad} oxidation [21, 22]. The results in Fig. 2(c) may confirm, on the other hand, that the diffusion of the molecule or ion is less constrained in SBA-15.

Figure 3 shows the MS-FTIR spectra of CO adsorbed on Pt-SBA-15/GC electrode in 0.1 M H_2SO_4 solution. E_S was varied from −0.30 V to 0.10 V, in which CO_{ad} species are stable. E_R was set at 1.00 V, where CO_{ad} species are oxidized to form CO_2. Three IR bands could be observed. The negative-going bands around 2,055 cm^{-1} and 1,850 cm^{-1} are assigned to IR absorption of linearly bonded CO (CO_L) and bridge bonded CO (CO_B) at E_S, respectively. Besides the CO_L and CO_B bands, a positive-going band near 2,345 cm^{-1} is ascribed to IR absorption of CO_2 species that were derived from the oxidation of CO_{ad} at E_R. In comparison with the IR adsorption of CO_{ad} on a bulk Pt electrode, a supplementary CO_B IR band is observed on Pt-SBA-15/GC electrode due to the enhanced IR adsorption (EIRA) phenomenon [21, 23]. To evaluate quantitatively the effect of IR enhancement absorption

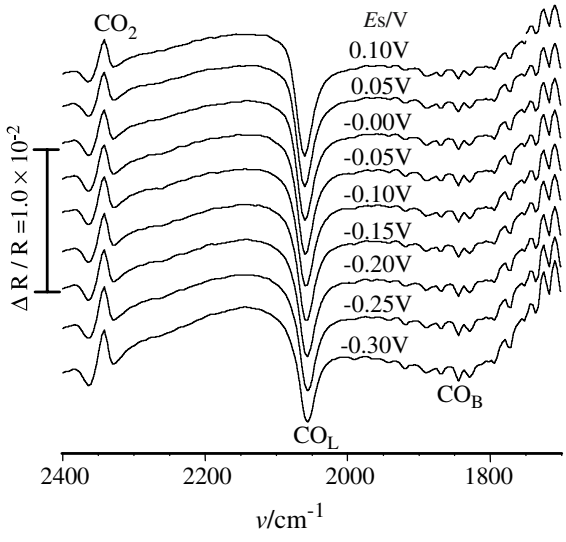

Fig. 3 In situ MS-FTIR spectra of CO adsorbed on Pt-SBA-15/GC in 0.1 M H_2SO_4. $E_R = 1.00$ V, E_S is indicated for each spectra

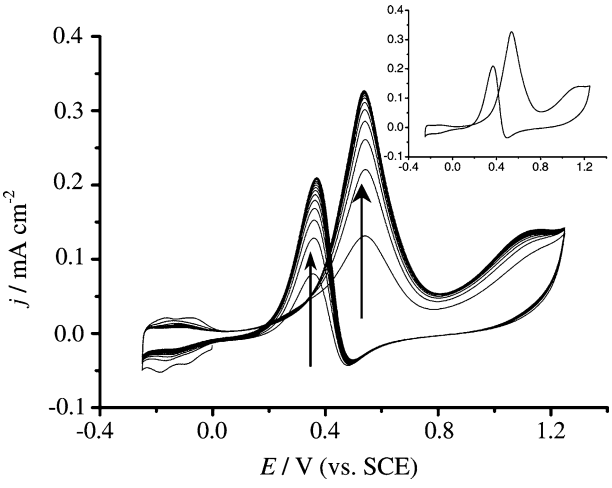

Fig. 4 The growing cyclic voltammograms of the newly prepared Pt-SBA-15/GC in 0.1 M H_2SO_4 + 0.05 M CH_3OH solution, sweep rate 50 mV s^{-1}. *Inset* is the stable voltammogram

on Pt-SBA-15/GC electrode, we define an enhancement factor (Δ_{IR}) that is equal to the ratio of the normalized CO_{ad} intensity on the Pt-SBA-15/GC electrode versus that on a bulk Pt electrode, i.e.,

$$\Delta IR = \frac{(NA_{CO_{ad}})Pt - SBA{-}15/GC}{(NA_{CO_{ad}})Pt} = \frac{A^{CO_{ad}}_{Pt-SBA-15/GC}}{A^{CO_2}_{Pt-SBA-15/GC}} \Big/ \frac{A^{CO_{ad}}_{Pt}}{A^{CO_2}_{Pt}} \quad (2)$$

where $A^{CO_{ad}}_{Pt-SBA-15/GC}$ and $A^{CO_2}_{Pt-SBA-15/GC}$ refer to integrated intensities of the CO_{ad} ($CO_L + CO_B$) and CO_2 IR bands, respectively, measured in IR spectra of Pt-SBA-15/GC electrode from Fig. 3; $A^{CO_{ad}}_{Pt}$ and $A^{CO_2}_{Pt}$ are the integrated intensities of the CO_{ad} (CO_L) and CO_2 bands, respectively, acquired from the IR spectra of a bulk Pt electrode [23]. From Eq. 2, the calculated Δ_{IR} equals 11, indicating that IR absorption of CO_{ad} has been enhanced 11 times on Pt-SBA-15/GC electrode. Besides the enhancement of IR absorption of CO_{ad}, the CO_{ad} bands are broadened on Pt-SBA-15/GC. The value of the full width at half-maximum (FWHM) of the CO_L band in Fig. 4 is measured to be 28 cm^{-1}, which is 13 cm^{-1} broader than that measured from the spectrum of a bulk Pt electrode (15 cm^{-1}) [23]. The EIRA is ascribed to the nanometer scale effect of Pt nanoparticles and also to the particular environment of CO_{ad}–Pt system that is confined in the channel of SBA-15.

It is well known that the "self-poisoning" phenomenon in electrocatalytic oxidation of small organic molecules is a fundamental subject in electrocatalysis field. This phenomenon is due to carbonyl intermediates formed by a spontaneous dissociation process, denoted the poisoning intermediates or poison. The carbonyl intermediates will be oxidized into CO_2 in the presence of active oxide species, which is formed at a relative high potential for a Pt polycrystalline electrode. Since both CO_{ad} can be easily oxidized and the IR absorption of CO_{ad} is enhanced on Pt-SBA-15/GC electrode, it is preferable to study the methanol oxidation on Pt-SBA-15/GC electrode.

Electrocatalytic oxidation of methanol

Studies of cyclic voltammetry

Potential cyclic scanning at a scan rate of 50 mV s^{-1} was carried out on a newly prepared Pt-SBA-15/GC electrode in 0.1 M H_2SO_4 containing 0.05 M CH_3OH solution, and the CVs are shown in Fig. 4. It can be seen that the current density of methanol oxidation increases progressively with the increase in the number of potential cyclic scanning, and the peak current density reaches stable values after about ten cycles, as shown in the inset. On the contrary, the redox peaks appearing at −0.20 V to 0.05 V, which is the characteristic of hydrogen adsorption–desorption, decrease gradually along with the increase in the scanning number. The phenomenon illustrates that the three processes, i.e., adsorption of methanol, dissociative adsorption of methanol, and adsorption–desorption of hydrogen, are competitive to each other on Pt-SBA-15/GC electrode [24, 25], and the surface structure may become favorable to the adsorption and the oxidation of methanol during the continuous potential cyclic scanning. It can be observed that the current begins to increase rapidly just above 0.15 V, and an oxidation peak appears at around 0.53 V in the PGPS. This oxidation peak is assigned to the oxidation of both reactive intermediates, referred to as the direct oxidation of methanol, and the poisoning species derived from methanol dissociative adsorption. In the negative-going potential sweep (NGPS), an oxidation current peak attributed to the direct oxidation of methanol emerges at about 0.36 V, right after a small reduction

peak appearing at 0.45 V. It is worth mentioning that the peak potential of methanol oxidation in the PGPS shifts negatively by about 0.10 V as compared to the Pt modified polymer electrodes [5, 7], indicating that the Pt-SBA-15/GC electrode exhibits high electrocatalytic activity for methanol oxidation. The description of the oxidation peak and the possible mechanism are interpreted in detail elsewhere [26, 27], which emphasized the effect of the diversified Pt oxide on the characteristic of the methanol oxidation.

In order to further reveal the correlation between methanol oxidation and Pt oxide species, we have studied the effect of upper limit potentials (E_U) in cyclic potential scanning on the methanol oxidation. Figure 5 shows typical CV curve of methanol oxidation on the Pt-SBA-15/GC electrode for E_U of 0.80 V. In this upper limit potential, the Pt oxides with high valence haven't developed greatly, so the effect of the Pt oxides with high valence on methanol oxidation in the NGPS is comparatively small. It can be seen that the potential of methanol oxidation peak remains invariable in the PGPS, while the potential of methanol oxidation peak shifts positively by about 0.06 V in the NGPS and the peak current density is almost equal to that in the PGPS. The fact that the current density of methanol oxidation in the NGPS and the PGPS are almost equal, illustrates that the methanol oxidation in the PGPS mainly takes place via the path of direct oxidation, and the dissociative adsorption of methanol on Pt-SBA-15/GC electrode, i.e., the "self-poisoning" phenomenon may be negligible. For comparison, the CV curve obtained on a Pt polycrystalline electrode in the close potential range, reported in literature [28], shows a different case. The current density of methanol oxidation in the PGPS was much higher than that in the NGPS due to the oxidation of dissociative adsorption species in the PGPS, and the total current density of methanol oxidation dramatically decreased with the increase in the number of potential cyclic scanning [28], indicating that the dissociative adsorption of methanol can easily occur on a Pt polycrystalline electrode.

Studies of programmed potential step

Figure 6 shows the comparison of $j \sim t$ curves for methanol oxidation on Pt-SBA-15/GC electrode and on a Pt polycrystalline electrode at 0.50 V. It can be seen that the methanol oxidation current on Pt polycrystalline electrode decays rapidly with the time, and the current in j–t curve is almost zero after 400 s. The rapid current decay has been interpreted as the "self-poisoning" of the adsorbed species derived from the dissociative adsorption of methanol [1, 28]. Correspondingly, the current density of methanol oxidation on Pt-SBA-15/GC electrode decreases comparatively slowly. When the time is above 400 s, the current density reaches a relatively stable value, which is still about one-sixth of the initial current density. It is obvious that the Pt-SBA-15/GC electrode exhibits a higher electrocatalytic activity and stability toward methanol oxidation.

In order to further measure the intrinsic electrocatalytic activity of Pt-SBA-15/GC electrode for methanol oxidation we have designed a program of potential steps. As shown in the inset to Fig. 7, the procedure contains three steps: (1) the electrode potential was first set at 0.75 V and held for 1 s to remove all possible adsorbates except Pt oxide formed at this potential; (2) the potential was then stepped negative to −0.20 V, and kept at this potential for 2 s to reduce Pt oxide and achieve the equilibrium of the reaction system; (3) finally, the potential was stepped to oxidation potential E_{ox} and $j \sim t$ data were recorded immediately. In order to achieve the same initial state of electrode, first several

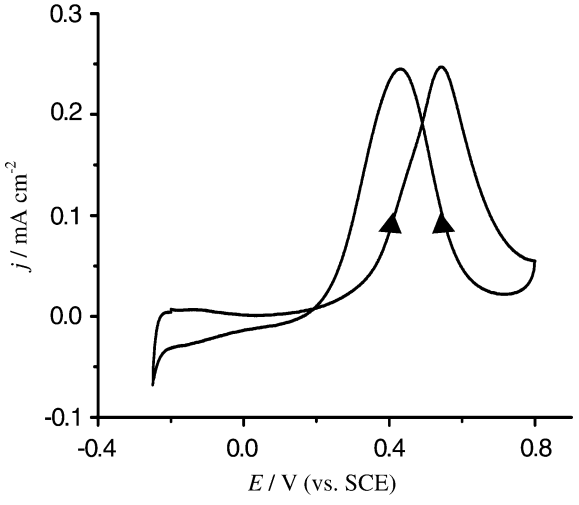

Fig. 5 Cyclic voltammogram of Pt-SBA-15/GC in 0.1 M H_2SO_4 + 0.05 M CH_3OH solution, sweep rate 50 mV s^{-1}, potential range −0.25–0.8 V

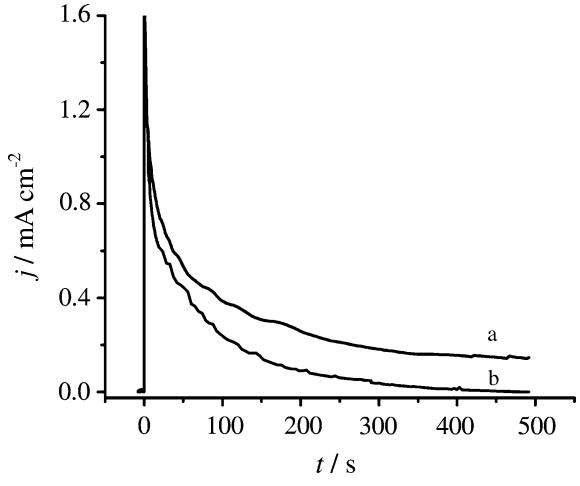

Fig. 6 $j \sim t$ Transients for methanol oxidation on **a** Pt-SBA-15/GC, **b** a Pt polycrystalline bead electrode in 0.1 M H_2SO_4 + 0.05 M CH_3OH solution. E_{ox} = 0.5 V

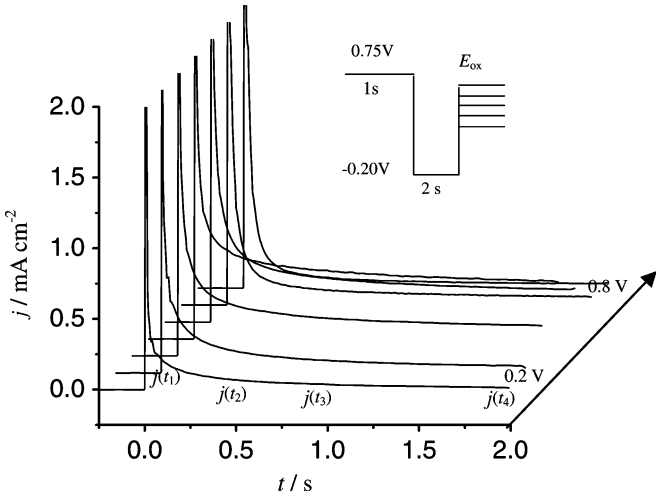

Fig. 7 A selected 3-D plot of j~t transients for methanol oxidation on Pt-SBA-15/GC in 0.1 M H_2SO_4 + 0.05 M CH_3OH solution. E_{ox} varied from 0.20 V to 0.80 V

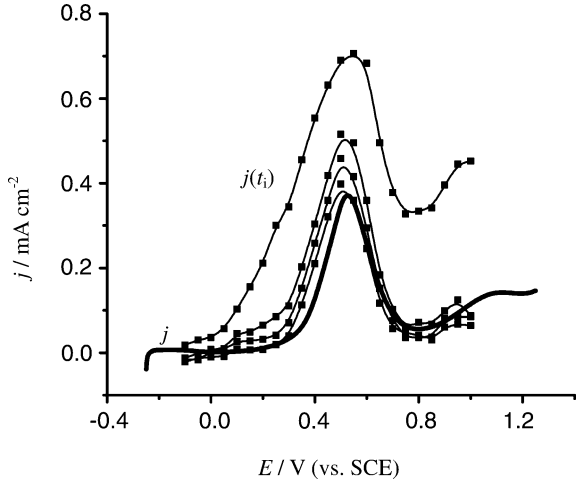

Fig. 8 Comparison of j (t_i)~E and j~E relationship on Pt-SBA-15/GC in 0.1 M H_2SO_4 + 0.05 M CH_3OH solution. j (t_i) measured at t = 0.1, 0.5, 1.0, 2.0 s (from top to bottom) from j~t transients for a given E_{ox} in Fig. 7, and j~E curve recorded in PGPS at a scan rate of 50 mV s^{-1}

potential cyclic scannings were carried out before the potential step program was applied. Hardly any methanol dissociated at −0.20 V for a stay of 2 s after stepping from a high potential. This programmed potential step procedure can ensure that the oxidation of methanol at E_{ox} takes place on a clean surface of the Pt-SBA-15/GC electrode without poisoning intermediate. A series of programmed potential step experiments were carried out by varying the oxidation potential E_{OX}. The selected j~t transient curves of methanol oxidation on the Pt-SBA-15/GC electrode at a series of E_{ox} are displayed in Fig. 7 in a three-dimensional presentation. We observe that the amplitude of j~t transients follows a parabolic variation and yield a maximum at around 0.50 V with the oxidation potential E_{ox} increasing gradually from 0.20 V to 0.80 V. It is interesting to sample the j~t curves of Fig. 7, i.e., taking the values of j at different t_i. The sampling data were denoted as j (t_i). Therefore, the plot of j (t_i) versus oxidation potential E_{ox} represents, in fact, the variation of intrinsic electrocatalytic activity of Pt-SBA-15/GC electrode for methanol oxidation at different potential. Figure 8 shows the comparison of j (t_i)~E curves with j~E curve recorded in the PGPS for methanol oxidation on Pt-SBA-15/GC electrode. It can be seen clearly that the onset potential of methanol oxidation is about 0.15 V. The j (t_i = 0.1 s)~E curve was significant high in comparison with other j (t_i)~E curves as well as the j~E curve. The decaying of j with t in the transient curves may be ascribed to the following two factors: the first is the effect of the double layer charging. The transient current will decrease quickly during the double layer charging. The second is the effect of the methanol diffusion, particularly the methanol diffusion into the channels of SBA-15. When the original adsorbed methanol on the electrode is consumed, it results in a big current decay. Since j (t_i = 2 s) has reached a relative steady current shown in the curve in Fig. 7, it may be appropriate to take the value of j (t_i = 2 s) in comparison with j~E curve. It can be seen from Fig. 8 that the j~E curve and j (t = 2 s) ~ E curve can inosculate each other well, which is evaluated by peak potential and peak current density, respectively. So the j~E curve shown in Fig. 8 may reflect the intrinsic electrochemical properties of Pt-SBA-15/GC electrode for methanol oxidation at different potential, where the effect of methanol dissociative adsorption can be negligible, and the j~E curves obtained in a continuous potential cyclic scanning may be considered as the quasi-stable activity of Pt-SBA-15/GC electrode for methanol oxidation.

Studies of in situ FTIR reflection spectroscopy

In order to characterize the nature of methanol oxidation on the Pt-SBA-15/GC electrode, in situ FTIRS studies were carried out. Fig. 9 shows a series of spectra on Pt-SBA-15/GC electrode in 0.1 M H_2SO_4 containing 0.05 M CH_3OH solution at different E_S varying from −0.10 V to 0.30 V. The reference potential E_R was set at −0.20 V, which is below the onset potential of methanol oxidation. Since the methanol concentration in the thin layer may decay gradually with its consumption during the spectra collection, we have modified the procedure of spectra collection on the basis of MS-FTIR procedure, which consists of a series of SPA-FTIR (single potential alteration FTIR) [29]: (1) a set of single-beam spectra of $R(E_R)$ at −0.2 V and $R(E_S)$ at E_{S1} was collected; (2) the electrode was lifted to renew the thin layer solution, and a set of other single-beam spectra of $R(E_R)$ at −0.2 V and $R(E_S)$ at E_{S2} was collected; (3) the procedure of (2) was repeated except that the E_{Si} was set at a new value. The result spectra were calculated by using Eq. 1 and is displayed in Fig. 9. A negative-going peak at 2,345 cm^{-1} is

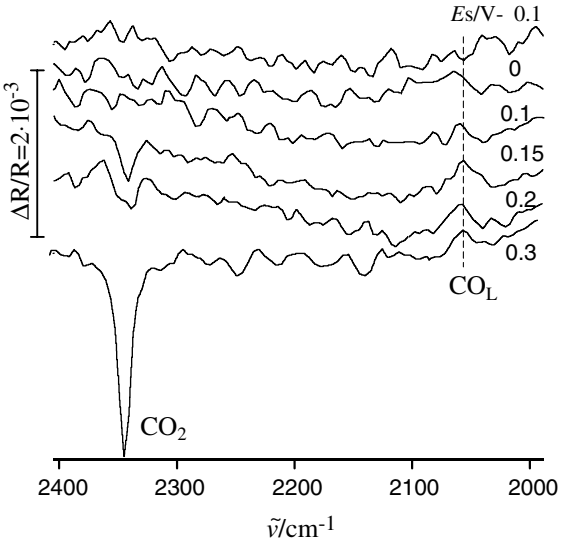

Fig. 9 In situ FTIR spectra of methanol oxidation on Pt-SBA-15/GC in 0.1 M H_2SO_4 + 0.05 M CH_3OH solution. $E_R = -0.2$ V, E_S is indicated for each spectra

observed when E_S reaches 0.15 V, the intensity increases further with increasing E_S. This IR band is assigned to IR absorption of CO_2 that is derived from methanol oxidation. The results indicate that the onset potential of methanol oxidation is near 0.15 V, which is basically in accordance with the results of CV and programmed potential step studies. In comparison with Pt deposited on Au electrode [30], the onset potential of methanol oxidation on Pt-SBA-15/GC electrode is ahead by approximately 0.20 V, signifying the high electrocatalytic activity of Pt-SBA-15/GC electrode for methanol oxidation. In addition, a weak positive-going band near 2,050 cm^{-1} ascribed to IR adsorption of CO_L can be observed for E_S above 0.10 V. According to Eq. 1, a positive going band is ascribed to the loss of IR absorption at E_{Si} in the case of a fixed E_R, which suggests that the CO_L, the only intermediate derived from methanol, can exist stably between -0.20 V ~ 0.10 V. Though the IR absorption of CO_L on Pt-SBA-15/GC electrode has been enhanced about 11 times as shown in Fig. 3, the intensity of CO_L derived from methanol is still very weak, indicating that methanol on Pt-SBA-15/GC electrode is comparatively difficult to dissociate and the intermediate thus formed can easily be removed. For comparison, methanol can be easily dissociated to form stable poisoning carbonyl species on bulk Pt and some Pt modified electrodes [26, 27]. It is well known that both the dissociative adsorption and the oxidation of methanol depend strongly on the surface structure of electrode. The SBA-15 silica could provide active oxygen species (Si–OH) surrounding Pt nanoparticles [31] .The results demonstrate that the formation of the poisoning CO species is suppressed on Pt-SBA-15/GC electrode to a large extent. Even if the intermediates form, they are oxidized easily by the aid of the active oxygen in SBA-15 silica. This can interpret the high electrocatalytic activity and stability of Pt-SBA-15/GC electrode toward methanol oxidation.

Conclusions

In this paper, the mesoporous SBA-15 silica was used as a nanoreactor to synthesize Pt nanoparticles that were prepared through impregnation and following calcinations, ultimately served to prepare a Pt-SBA-15/GC electrode. The onset potential of CO_{ad} oxidation appears at about 0.10 V. The channels with active silicon–hydroxyl in the SBA-15 apparently exhibit less resistance to molecular diffusion and electric charge transfer in CO_{ad} oxidation, resulting in the easy oxidation of CO_{ad}. Enhanced infrared absorption (EIRA) of Pt nanoparticles confined in SBA-15 for CO adsorption was observed by in situ FTIR spectroscopy studies, consisting of the enhancement of IR adsorption (enhanced 11-fold) and broadening of the CO_{ad} bandwidth (broadened 13 cm^{-1}).

The onset potential of methanol oxidation on Pt-SBA-15/GC electrode is seen at about 0.15 V. The chronoamperometry results discovered that Pt-SBA-15/GC electrode possesses a higher electrocatalytic stability toward methanol oxidation than Pt polycrystalline electrode. In situ FTIRS results demonstrated that the linearly bonded CO (CO_L) is the only intermediate derived from methanol, which is suppressed on Pt-SBA-15/GC electrode to a large extent, and is more readily oxidized to form CO_2 as the final product of the methanol oxidation by the aid of the active oxide in SBA-15 silica system.

Acknowledgments This work was supported by the National Natural Science Foundation of China (90206039), the National Key Basic Research and Development Program (2002CB211804), Cooperation Program Between China and Russia (20411120147), and Technological Innovation Program of Xiamen University (XDKJCX20041012).

References

1. Leger JM, Lamy C (1990) Ber Bunsenges Phys Chem 94:1021
2. Frelink T, Visscher W, Van Veen JAR (1995) J Electroanal Chem 382:65
3. Liu L, Pu C, Viswanatha R, Fan Q, Liu R, Smotkin ES (1998) Electrochim Acta 43:3657
4. Schell M (1998) J Electroanal Chem 457:221
5. Golabi SM, Nozad A (2002) J Electroanal Chem 521:161
6. Yang H, Lu TH, Xue KH, Sun SG, Lu GQ, Chen SP (1997) J Electrochem Soc 144:2302
7. Yang H, Li CZ, Lu TH, Xue KH, Sun SG (1997) Acta Phys-Chim Sin 13:542
8. Zhao DY, Feng JL, Huo QS, Melosh N, Fredrichkson GH, Chmelka BF, Stucky GD (1998) Science 279:548
9. Kresge CT, Lonowicz MZ, Roth WJ (1992) Nature 359:710
10. Yue Y, Gedeon A, Bonardet J, D' Espinose J, Fraissard J, Melosh N (1999) Chem Commun 999:1967
11. Luan ZH, Hartmann M, Zhao D, Zhou W, Kevan L (1999) Chem Mater 11:1621

12. Wang Y, Noguchi M, Takahashi Y, Ohtsuka Y (2001) Catal Today 68:3
13. Yang W, Wang XX, Guo Q, Zhang QH, Wang Y (2003) New J Chem 27:1301
14. Lu GQ, Sun SG, Cai LR, Chen SP, Tian ZW, Shiu KK (2000) Langmuir 16:778
15. Bal L, Gao L, Conway BE (1993) J Chem Soc Faraday Trans 89:235
16. Hachkar M, Napporn T, Leger JM, Beden B, Lamy C (1996) Electrochim Acta 41:2721
17. Cherstiouk OV, Simonov PA, Zaikovskii VI, Savinova ER (2003) J Electroanal Chem 554–555:241
18. Funke HH, Frender KR, Green KM, Falconer JL (1997) J Membr Sci 129:77
19. Groen JC, Perez-Ramirez J (2004) Appl Catal A Gen 268:121
20. Ravikovitch PI, Neimark AV (2001) J Phys Chem B 105:6817
21. Jiang YX, Sun SG, Ding N (2001) Chem Phys Lett 344:463
22. Jiang YX, Ding N, Sun SG (2004) J Electroanal Chem 563:15
23. Chen W, Sun SG, Zhou ZY, Chen SP (2003) J Phys Chem B 107:9808
24. Li NH, Sun SG (1998) J Electroanal Chem 448:5
25. Beden B, Hahn F, Leger JM (1991) J Electroanal Chem 301:129
26. Wasmus S, Küver A (1999) J Electroanal Chem 461:14
27. Iwasita T (2002) Electrochim Acta 47:3663
28. Sun SG, Lipkowski J, Altounian Z (1990) J Electrochem Soc 137:2443
29. Corrigan DS, Legung LWH, Weaver MJ (1987) Anal Chem 59:2252
30. Shen P, Chen K, Tseung C (1994) J Chem Soc Faraday Trans 90:3089
31. Guo C, Zhang D, Jin GX (2004) Chin Sci Bull (in English) 49:249